

Contents lists available at ScienceDirect

# Colloids and Surfaces A: Physicochemical and Engineering Aspects



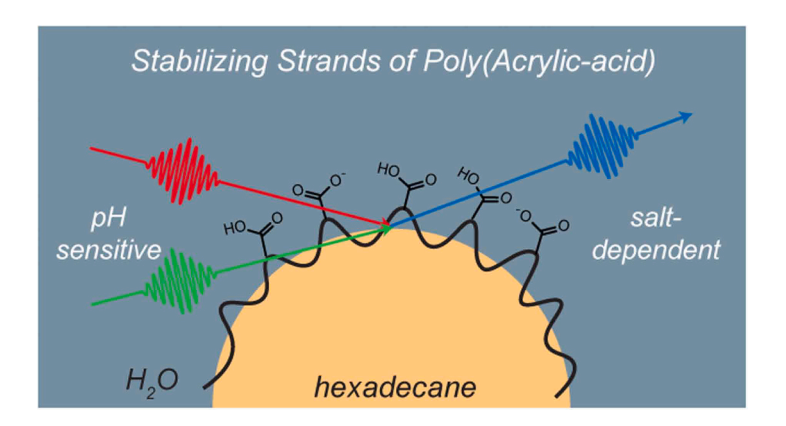
journal homepage: www.elsevier.com/locate/colsurfa

# Stabilizing strands: Exploring the kinetic stability of polymer-coated emulsions with surface specific spectroscopy

Ashley N. Mapile<sup>1</sup>, Lawrence F. Scatena<sup>\*,2</sup>

Department of Chemistry and Biochemistry. University of Oregon, Eugene, OR 97403, United States

G R A P H I C A L A B S T R A C T



## ARTICLE INFO

Keywords:
Emulsion stability
Polyelectrolyte adsorption
Poly(acrylic acid)
Vibrational sum frequency scattering
spectroscopy
Colloidal stability
Interfacial pH

#### ABSTRACT

Emulsions on the scale of 100 s of nm in diameter traditionally achieve long-term colloidal stability (> 1 month) through surfactants or a combination of surfactant and polymer. The stability of emulsions coated with only polyelectrolyte remains largely unknown. Here, we introduce an emulsion system coated with the surface-active polymer, poly(acrylic acid) (PAA) that stabilizes hexadecane-in-water emulsions with a marked dependence on pH and ionic strength. Surface specific vibrational sum frequency scattering spectroscopy (VSFSS) provides a molecular picture of PAA organization at the hexadecane-water droplet interface while dynamic light scattering and zeta potential measures the colloidal stability as a function of pH and salt concentration. We find that a steric layer of polymer alone stabilizes emulsions despite having a low zeta potential (<5 mV) suggesting a mechanism of stability unexplained by traditional theories. In fact, as the magnitude of the zeta potential increases, emulsions become polydisperse and unstable. VSFS spectra reveals that an ordered backbone at pH 2 and pH 4

Abbreviations: PAA, polyacrylic acid; VSFSS, vibrational sum frequency scattering spectroscopy; DLS, dynamic light scattering; PDI, polydispersity index; SFG, sum frequency generation.

E-mail address: scat@uoregon.edu (L.F. Scatena).

<sup>\*</sup> Corresponding author.

<sup>&</sup>lt;sup>1</sup> ORCID ID: 0000-0002-7808-4692

<sup>&</sup>lt;sup>2</sup> ORCID ID: 0000-0003-2466-8825

#### 1. Introduction

Small oil droplets (on the order of 100s of nm in diameter) suspended in aqueous solution require high energy mixing for formation and are thermodynamically unstable, resulting in phase separation over time [1-4]. Making kinetically stable emulsions and understanding the mechanism of oil droplet stability has far reaching implications, from the development and enhancement of new cosmetic products, to the efficacy of drug delivery systems and oil spill remediation formulations [5-7]. Traditionally, kinetically stable oil droplets with diameters of 20-200 nm are classified as nanoemulsions while larger droplets with diameters of 200-1000 nm in diameter can be referred to as miniemulsions [8]. Regardless of the size, surfactant-coated emulsions are useful laboratory analogues for modeling commercially-used dispersants that reduce the surface tension of a large oil patch and enable the formation of stable, small oil droplets that are continuously distributed by waves and eventually biodegraded by marine microbes [9]. Beyond oil remediation, the curved interface of emulsions have proven to be of interest to measure molecular packing behavior as compared to planar interfaces. The Richmond/Scatena lab and others have postulated that the geometry of the interface and the thermodynamic instability of emulsions are responsible for the observed differences in molecular orientation and conformation at the two interfaces [10-14].

While non-toxic surfactants are useful for environmental applications, the introduction of proteins as colloid stabilizers have the potential to encapsulate and selectively deliver hydrophobic drugs [15–19]. It is hypothesized that colloids are stabilized by protein coronas through steric hinderance or, in other words, a thick protein shell prevents droplets from coalescing. While recent work using 2D-IR spectroscopy and sum frequency scattering spectroscopy have investigated the newfound importance of protein-stabilized colloids, the molecular conformation and detailed mechanism of stability remain difficult to probe due to the complicated nature of long-chain proteins and their resulting coronas [20,21].

Polyelectrolytes are useful analogues for studying protein coronas as both macromolecules have varying functional groups along a repeating backbone, a nuanced folding or coiling structure with the ability to hydrogen bond or form secondary structures, and charge localization along the chain dictated by environmental pH. Yet, polyelectrolytes are often easier to study than proteins due to their known monomer units and simple tunability of molecular weight, percent protonation, and secondary structure. In addition to their pH-dependent behavior in bulk solution, acids and polyelectrolytes adsorbed at interfaces are known to have a surface  $pK_a \sim 1$  unit more alkaline than the bulk  $pK_a$  due to interfacial solvent dielectrics reducing the solvation energy of the acid functional groups [22–27]. This pH-dependence is critical for materials such as polyelectrolyte coarcervates, where stabilization across a variety of conditions can be a challenge [28,29]. Poly(acrylic acid) (PAA, Fig. 1 inset) is a simple polyelectrolyte that can mimic protein behavior at interfaces. PAA, which contains a single carboxylic acid repeating group, can expand in solution when deprotonated or hydrogen bond with itself to form coils when protonated and is a useful material in forming zwitterionic polymer coarcervates [30-34]. Through pH-dependent zeta potential measurements (see Supporting Information) the interfacial pKa of PAA at the hexadecane/water emulsion interface was determined to be ~5.3, about 0.8 units more alkaline than the bulk pK<sub>a</sub> (Fig. 1). Therefore, studying the pH-dependent conformational behavior of PAA adsorbed at the emulsion interface can provide insight into droplets stabilized by pH-sensitive protein coronas as well as a detailed understanding of the mechanisms of colloidal stability.

The adsorption behavior of PAA without the addition of a surfactant,

has been studied at both the planar CCl<sub>4</sub>/water and air/water interfaces using vibrational sum frequency spectroscopy (VSFS). These studies found that in conditions above the pKa (pH >4.5), the polymer is interfacially inactive, but the addition of charge-screening cations promotes adsorption of the polymer to the interface [11,35–38]. Below pH 4.5, the polymer is interfacially active and exhibits a well-ordered structure as evident by strong CH and C=O VSFS spectral features. At a planar interface, molecular dynamics are thermodynamically determined by equilibrium surface activity and surface-active molecules develop a stable configuration given time. On the other hand, emulsions require the input of external energy to form droplets resulting in a kinetically trapped interface [2,8]. During the formation of emulsions, surface-active molecules initially adsorb to the interface via ultrasonication but subsequently adsorb/desorb through equilibrium thermodynamics after formation of the curved interface. Thus, the conformational ordering of interfacial molecules adsorbed to emulsions is dictated by the thermodynamic equilibrium of molecular adsorption and the kinetic energy encouraging the platform of these colloids to destabilize and coalesce. Stabilization of emulsions is best described by the theory developed by Derjaguin, Landau, Verwey, and Overbeek (DLVO) which states that both electrostatic and steric repulsion prevents droplet coalescence and keeps the emulsions in a kinetically trapped state [2,8,39,40]. Reports of emulsions coated with solid polymer particles (such as Pickering emulsions) [41], nanoparticles with a polymeric coating [42], and emulsions formed with surfactant/polymer mixtures [43] suggest unique behavior at curved hydrophobic interfaces as opposed to their planar counterparts. While there have been reports of emulsions stabilized with polymer alone, observed through Janus particles [44] or magnetic nanoemulsions [45], and specifically emulsions coated with diblock copolymers [46,47], they lack insight into the detailed mechanism of stability promoted by polymers or the molecular level information to provide a structural understanding of the droplet interface.

Here, we demonstrate the stability of emulsions coated with PAA and provide a picture of polymer molecular conformation with the surface-specific vibrational sum frequency scattering spectroscopy (VSFSS). Despite the lack of surface charge thought to be necessary for droplet stabilization, PAA-coated emulsions prepared at pH 2 are stable and exhibit interfacial polymer ordering. Surprisingly, the highly charged pH 6 polymer does not stabilize emulsions and exhibits no molecular organization. With the addition of salt, we observe charge screening at the interface and a disruption to polymer ordering because of localized

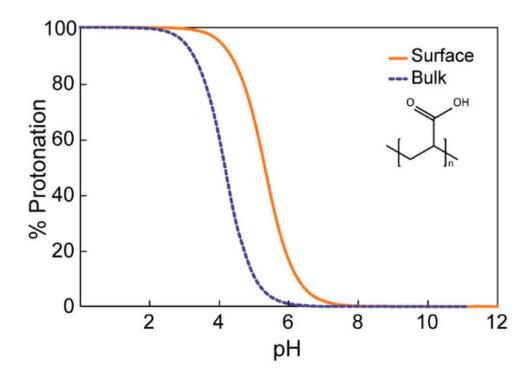


**Fig. 1.** Chemical structure of poly(acrylic acid) and percent protonation curve as a function of pH for surface (solid, orange line) and bulk (dotted, purple line). Percent protonation was calculated with the Henderson-Hasselbalch equation, the known bulk  $pK_a$  (4.5), and the experimentally derived interfacial  $pK_a$  (5.3).

electrostatics. We propose that emulsions are stabilized through the steric hindrance of an adsorbed PAA layer, whose molecular conformation and charge-dependent behavior can provide insight to protein corona-stabilized droplets and their application as drug delivery vehicles.

#### 2. Experimental

#### 2.1. Materials

All materials were used as delivered without further purification. Hexadecane ( $\geq 99$ %), dioctyl sodium sulfosuccinate (AOT,  $\geq 97$ %), poly(acrylic acid) (PAA, average  $M_v \sim 450,000$ ), calcium chloride (CaCl $_2$ , anhydrous,  $\geq 97$ %), magnesium chloride (MgCl $_2$ , anhydrous,  $\geq 98$ %), sodium chloride (NaCl, BioXtra,  $\geq 99.5$ %), and ammonium chloride (NH4Cl, ACS reagent,  $\geq 99.5$ %) were purchased from Sigma-Aldrich. Deuterated hexadecane (n-hexadecane-d $_34$ , 98.6% D), sodium deuteroxide (NaOD, 99.5% D), and deuterium chloride (DCl, 99.8% D) were purchased from CDN Isotopes. Deuterium oxide (D2O, 99.9% D) was purchased from Cambridge Isotope Labs. All glassware was copiously cleaned in a bath containing sulfuric acid (98% Sigma-Aldrich) and AlNOCHROMIX oxidizer from Godax Laboratories Inc. After sitting in the acid bath for at least 24 hours, glassware was rinsed for at least 2 min. with 18.2 M $\Omega$ -cm water and dried in an oven.

#### 2.2. Emulsion formation

Emulsions consisting of hexadecane (or d-hexadecane) suspended in water (or  $\mathrm{D}_2\mathrm{O}$ ) were prepared by ultrasonication (Branson Sonifier 250) of the sample at 5 % output power ( $\sim$ 12.5 %) at 20 kHz for 5 minutes at a constant duty cycle. The ultrasonication probe tip was placed at the interface of the aqueous solution and oil layer to ensure homogenous mixing. The AOT-coated emulsion standard was formed by ultrasonicating AOT stock solution with oil to give a 1 mM AOT emulsion with 2.5 % v/v oil in water. PAA-stabilized emulsions were formed in the same fashion with DCl or NaOD added to reach the desired pD (pH). Emulsion pH was measured using MilliporeSigma MColorpHast pH strips and an Oakton Instruments Portable Meter Kit. The detection of pH values can differ from pD values by 0.43 [48], however for ease of communication, pH is used in this paper.

#### 2.3. Dynamic light scattering and zeta potential

Emulsion hydrodynamic diameter (Z-average), polydispersity index (PDI), and zeta potential were measured by a Malvern Zetasizer Nano ZS. Details regarding the theory and practice of dynamic light scattering (DLS) and zeta potential can be found elsewhere [49,50]. From DLS measurements, hydrodynamic diameter and PDI was reported from an average of at least three measurements. DLS and zeta potential measurements were collected by pipetting 1 mL of emulsion solution into a Malvern folded capillary zeta cell, therefore maintaining consistent v/v oil concentrations. Zeta potential values were reported from an average of at least five measurements. Determination of the surface  $pK_a$  using zeta potential measurements is detailed in the Supporting Information (Figure S1) and follows a procedure developed by Haes  $\it et.~al.~[51]$ 

### 2.4. Vibrational sum frequency scattering spectroscopy

Vibrational sum frequency scattering spectroscopy (VSFSS) is a second-order non-linear spectroscopic technique that provides information on the population and molecular ordering at curved interfaces. Rigorous theory describing sum frequency generation (SFG) can be found elsewhere, but in general, symmetry considerations under the electric dipole approximation dictate that an SFG response is forbidden in bulk media and only occurs at a non-centrosymmetric environment, such as an interface [52,53]. The VSFSS experimental setup used here

has been described thoroughly in other publications from the Richmond/Scatena laboratory [14,54]. Briefly, a Ti:Sapphire regenerative amplifier laser (Coherent Libra) generates an 800 nm, ~80 fs fundamental pulses with a 1 kHz repetition rate. A portion of that beam is used as the visible pulse while the remaining is sent through an optical parametric amplifier (Coherent OPerA Solo) to generate a broadband infrared (IR) beam through difference frequency generation. The visible and IR pulses are then directed along a series of mirrors, lenses, and polarizers to become spatially and temporally overlapped at the sample stage. The sample cell is composed of a CaF2 window in the front and a quartz cuvette in the back (Helma QS) with an optical path length of  $200~\mu m.$  The IR beam is focused at the sample to a spot size of  ${\sim}80~\mu m$ with a parabolic gold mirror, while the visible beam is focused right after the sample cell to a  $\sim$ 500  $\mu$ m spot size. The scattered SFG response is collected at an angle of  $\sim 60^{\circ}$ , collimated with a plano-convex lens, and focused into a spectrograph and accompanying charge-coupled device intensifier (Princeton Instruments IsoPlane SCT320 and PI-MAX4). For all experiments, the visible pulse energy was 25 μJ while the IR pulse energies were 2-3 µJ and 5 µJ for the C=O and C-H stretching regions, respectively.

#### 2.5. Data analysis and spectral fitting

To account for daily fluctuations in laser power, a single trace in a figure is the result of at least 3 averaged trials across different days. One trial consists of 2 signal and 2 background measurements. Each trial is averaged, background subtracted, and normalized by a non-resonant response from KNbO3 to account for changes in IR spectral shape. In the C-H region, spectra are further normalized by the integrated SFG intensity (from 2800 to 3000 cm $^{-1}$ ) generated from a d-hexadecane emulsion in  $\rm D_2O$  stabilized with 1 mM AOT. Each trial is further normalized by the size of the droplet (determined by a monomodal distribution from DLS) through a scattering pattern developed by Roke et. al. that accounts for the percentage of scattered signal collected at 60° which is dependent on droplet size and beam polarizations [55,56]. More details on the normalization procedure for VSFSS utilized in the Richmond/Scatena laboratory can be seen in a previous publication [54].

In VSFSS, the intensity of the scattered SF response is proportional to the intensities of the incoming visible and IR beams  $(I_{IR}I_{vis})$  and the square modulus of the second-order nonlinear susceptibility  $(X^{(2)})$ . The  $X^{(2)}$  has non-resonant and resonant terms which are accounted for in the fitting Eq. (1) as developed by Bain  $et\ al.$ 

$$|X(\omega)^{(2)}|^2 = \left| X_{NR}^{(2)} e^{i\phi} + \sum_{\nu} \int_{-\infty}^{+\infty} \frac{A_{\nu} e^{i\phi\nu} e^{-\left(\frac{\omega_L - \omega_{\nu}}{\Gamma_{\nu}}\right)^2}}{\omega_L - \omega_{IR} + i\Gamma_L} d\omega_L \right|^2$$
(1)

where the amplitude of the non-resonant susceptibility is described by  $X_{NR}^{(2)}$  with a phase  $\phi$  [57]. The summation of all vibrational transitions that are SFG active describes the resonant susceptibility, where  $A_{\nu}$  is the peak amplitude,  $\phi$  is the phase,  $\Gamma_L$  is the Lorentzian linewidth describing homogenous broadening, and  $\Gamma_{\nu}$  is the Gaussian linewidth describing inhomogeneous broadening. Eq. 1 is used to fit all experimental spectra. Tables S2-S7 list the fitting parameters used in this paper.

## 3. Results and discussion

## 3.1. Impact of PAA concentration

Emulsions were formed with concentrations of PAA ranging from 1 ppm to 4000 ppm in the natural pH conditions of PAA (pH 4) and measured by dynamic light scattering and zeta potential (Fig. 2). For context, previous experiments at the CCl<sub>4</sub>/water interface used 5 ppm

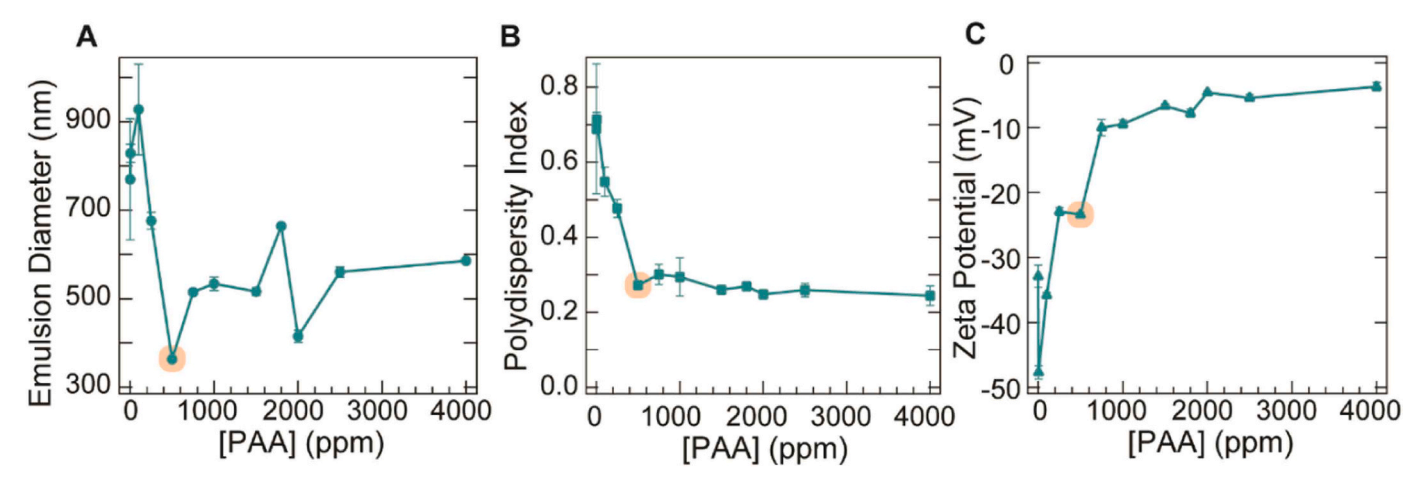


Fig. 2. Characteristics (hydrodynamic diameter, polydispersity index, and zeta potential) of emulsions coated with varying amounts of PAA at pH 4. Points shaded orange indicate 500 ppm PAA.

PAA while air/water interface experiments used 4500 ppm [11,35]. Figure S2 and Table S1 demonstrate that emulsions prepared at or below 250 ppm PAA were unstable after 1 week. Bare emulsions (those without deliberately added surface active agents) are known to have a negative zeta potential due to miniscule amounts of surface active contaminants [58,59]. The zeta potential of our hexadecane/water emulsions (-32 mV) suggest minor surface active impurities. The presence of these impurities were identified in previous emulsion studies from our laboratory that employed meticulous and extensive cleaning procedures to minimize their presence [59]. After PAA addition, the polymer is much more surface active than the impurities and displaces any contaminants that contributed to the negative surface charge. As additional PAA is added, charge screening and hydrogen bonding causes a reduction in the magnitude of the zeta potential.

At a concentration of 500 ppm, PAA-stabilized emulsions exhibit good colloidal stability, moderately polydisperse size distributions, and a highly charged surface layer as indicated by the orange shaded points in Fig. 2. Additionally, as confirmed by pendant drop surface tensiometery, discussed in the Supporting Information and Figure S3, PAA adsorbs to the hexadecane/water interface at a concentration of 500 ppm. Emulsions formed using 250 ppm PAA and below resulted in unstable droplets presumably due to a lack of surface population. Despite a remarkably high magnitude zeta potential (>30 mV) emulsions stabilized with 100 ppm PAA or below are unstable and crash out quickly after formation, likely due to a thin or completely absent polymer layer. While the addition of PAA at concentrations above 500 ppm leads to more stable emulsions, as indicated by the long-term stability, significant charge screening occurs making them difficult targets for measuring the interplay between electrostatics and steric repulsion when salt ions are added. The slight increase in emulsion size and reduction in zeta potential with increasing concentration of PAA is due to polymer layering at the surface which extends the hydrodynamic diameter and charge screens the surface as is consistent with other polymer-layering studies [46,60-62]. Emulsions stabilized with 1500 ppm PAA or higher have a low zeta potential (~-7 mV) and are colloidally stable up to a week, solidifying the observation that sterics alone are enough to stabilize emulsions. Due to the desire to study the impact of surface charge screening, the emulsions used in this paper are formed with 500 ppm PAA as they have long-term colloidal stability, are moderately polydisperse and have appreciable interfacial charge.

## 3.2. Emulsions stabilized by PAA alone

Emulsions coated with 500 ppm PAA were formed at pH 2, pH 4, and pH 6 via ultrasonication of 2.5 % v/v hexadecane in water. Pendant drop surface tensiometery measurements indicate that high amounts of

PAA adsorb to the hexadecane/water interface at pH 2 and pH 4 while little adsorption is observed at pH 6 (Figure S3). Emulsions at pH 2 and pH 4 maintained colloidal stability after one week, as evident by their visual turbidity, while pH 6 oil droplets phase separated (Figure S4). Dynamic light scattering of pH 2, pH 4, and pH 6 colloids measured 20 minutes after formation revealed hydrodynamic diameters of 477.7, 363.2, and 761.0 nm, respectively, demonstrating that the average size of emulsions prepared at pH 2 and 4 are in the nanosized regime while pH 6 emulsions are inherently larger. Narrow, monodisperse colloids have a PDI < 0.1, while polydisperse systems have a PDI > 0.1 [63]. Moderate polydispersity is defined by a PDI from 0.1 to 0.4 and describes the pH 2 and pH 4 emulsions studied here (PDIs of 0.247 and 0.272, respectively), while the pH 6 emulsions have broad polydispersity (PDI of 0.628). Similarly, size distribution plots from DLS measurements are monomodal for emulsions at pH 2 and pH 4, but multimodal for pH 6 (Figure S5). Table S2 lists the PDI of each emulsions system studied by VSFSS which are in line with recent studies on emulsion formulations [46,64-66]. To be acceptable for drug delivery applications, monodisperse colloids are defined to have a PDI < 0.3 while polydisperse systems have a PDI > 0.3, however stricter criterion of monodispersity may require a PDI < 0.1 [8,67,68]. The zeta potential of pH 2 emulsions was measured to be only -3.08 mV, while at pH 4 zeta potential measurements reveal a charge of -23.4 mV. At only 16.7 % protonation of PAA at pH 6 (Fig. 1), oil droplets have a significantly charged interface with a zeta potential -45.0 mV. Doping-in acid or base to an emulsion initially prepared at the natural conditions (pH 4) has little impact on the resulting size, PDI, or zeta potential of pH 2 or pH 4 droplets (Figure S6) suggesting that emulsion stability is pH reversible and dependent on polymer adsorption.

The long-term stability of emulsions prepared at pH 2 is remarkable considering that polymers and surfactants/salt or post-functionalized emulsions are typically required to stabilize emulsion oil droplets due to the necessity of interfacial charge [69-71]. For example, reports of low-charge emulsions such as those coated by the surfactant sodium decanoate in acidic conditions, have a zeta potential of about -5 mV and destabilize within one hour [14]. The appreciable change in zeta potential can be attributed to the ~5 % of deprotonation difference between PAA at pH 2 (~99.9 % protonated) and pH 4 (~95.2 % protonated). The instability of the pH 6 oil droplets is surprising considering that the degree of zeta potential for these droplets is similar to that experienced by hexadecane-in-water emulsions stabilized with 10 mM sodium decanoate where the zeta potential is about -50 mV [14]. Due to this strong electrostatic repulsion, decanoate-stabilized emulsions can be stable upwards of months with slight Ostwald ripening. The stability of this PAA-coated emulsion system contradicts what is displayed by surfactant-stabilized emulsions, thus, we examine this system with

VSFSS to gain a molecular-level understanding of the polymer conformation at the emulsion interface that gives rise to this unique colloid stability.

VSFSS spectra of the colloids coated with PAA in pH 2, pH 4, and pH conditions were measured in the C-H stretching region (2800–3000  $\mbox{cm}^{-1}\mbox{)}.$  Two major peaks were observed at pH 2 and pH 4 while no signal was measured for pH 6 (Fig. 3A). In accordance with previous heterodyne-detected SFG experiments at the planar air/water interface, as well as complementary bulk IR and Raman spectroscopies, the broad feature at  $2877~\mathrm{cm}^{-1}$  is assigned to the methine (CH) stretch and the feature at 2929 cm<sup>-1</sup> is assigned to the methylene (CH<sub>2</sub>) symmetric stretch [11,72]. The higher frequency feature also contains contributions from the methylene asymmetric overtone and Fermi Resonance [11]. The broad full width at half maximum present in the methine stretch at pH 4 (53 cm<sup>-1</sup> and 16 cm<sup>-1</sup> for the methine and methylene stretch, respectively) can be attributed to different solvation environments for the CH mode that is tethered to the carbonyl group [73]. At pH 4, methylene modes presumably lie strictly in the oil phase while the carbonyl groups pull the methine modes further away from the interface, comparable to what was observed to poly(methacrylic) acid at the planar CCl<sub>4</sub>/water interface [74]. The variety of oil- and water-solvated environments of the methine results in the peak broadening. At pH 2, the methine feature is nearly absent. SFG experiments hydrolyzed polyacrylamide (HPAM) Fourier-transform IR spectra of PAA show an increase in the CH2 intensity while the CH feature broadens and decreases in intensity with increasing amount of polymer due to a higher population of methine modes being solvated in the water phase [72,73]. For PAA, as more polymer saturates the interface from pH 4 to pH 2, as indicated by the increase in surface pressure (Figure S3), it is likely that some of the methine CH modes are solvated in the oil while others are solvated in the water.

At pH 4, the presence of two distinct and high intensity CH modes suggests that the polymer adopts a conformation at the interface with a well-ordered backbone. At pH 2 the methine stretch is nearly absent and the methylene stretch is reduced, suggesting a less ordered conformation of PAA as compared to pH 4. These differences in signal intensity can be explained as the result of slight differences in polymer organization and protonation. At pH 2, PAA is  $\sim$ 99.9 % protonated at the interface while at pH 4 PAA is  $\sim$ 95.2 % protonated (Fig. 1). While the  $\sim$ 5 % difference

in protonation might seem insignificant, it has been observed that uncharged polyelectrolytes in bulk aqueous environments develop a random coil conformation [30]. This coiling is promoted by acidic conditions where intramolecular H-bonding between carboxylic acid moieties is most favorable. Extending this behavior to the interface, where the interfacial pKa of 5.3 (as compared to the bulk pKa of 4.5) promotes the formation of acidic polymer (Fig. 1), the decrease in polymer backbone signal moving to acidic conditions is attributed to random coiling of polymer and forming intramolecular hydrogen bonds at the interface [11]. At pH 2, decreasing the persistence length of the polymer through coiling is thermodynamically favorable and akin to protein folding, in which the hydrophobic moieties favor intramolecular hydrogen bonding as opposed to aqueous solvation. In contrast, oil droplets prepared at pH 6 have PAA molecules that are  $\sim\!\!16.7~\%$  protonated. It has been observed in bulk aqueous solutions that as ionization of a carboxylic acid polymers increases, the persistence length increases [32,75]. In a similar fashion to a protein unfolding, uncoiling of the highly charged polymer allows for charge solvation within the aqueous phase. While our experiments cannot conclusively determine the location of PAA at pH 6, we hypothesize that the polymer is either located near the interface (within the boundaries of a solvation shell) or at the interface in a low or disordered population. While the lack of signal observed for PAA at pH 6 could be attributed to the extended polymer solvated in the aqueous phase, as in previous SF experiments of PAA at the planar CCl<sub>4</sub>/water interface, the surface pressure and high magnitude negative zeta potential measurements suggests that PAA is near the oil droplet surface. Therefore, we will assume that at pH 6, PAA has minimal ordered surface population resulting in the absence of VSFSS signal.

The pendant groups of PAA were also measured by VSFSS in the C=O stretching region (Fig. 3B) to determine the orientation of the pH-sensitive functional groups at pH 2 and pH 4. Experimentally, a large non-resonant background is experienced in the C=O region, likely due to the CaF<sub>2</sub> window [14,76]. De-timing of the visible beam is used to reduce the non-resonant response, however, weak C=O signals also reduce in intensity and result in noisy spectra in this region. A small feature is seen in the C=O region for pH 4 at 1735 cm<sup>-1</sup> assigned to the C=O stretching mode on the polymer pendant group consistent with VSFS experiments of PAA at the CCl<sub>4</sub>/water interface [37]. Data from PAA-coated oil droplets at pH 6 is omitted from this graph for clarity, as

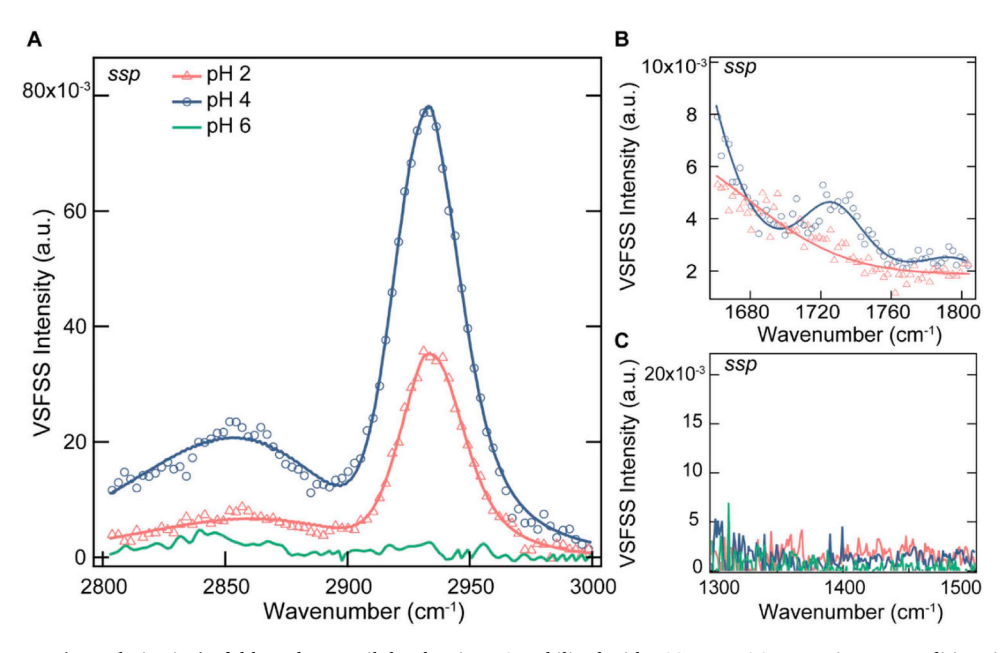


Fig. 3. VSFSS measurements (ssp polarization) of d-hexadecane oil droplets in  $D_2O$  stabilized with 500 ppm PAA at varying pH conditions in the A) C-H stretching region, B) carbonyl (C=O) stretching region, and C) the carboxylate (COO-) symmetric stretching region. Solid lines represent fits of the data.

the signal resembled the non-resonant background exhibited at pH 2. The absence of a C=O vibrational mode at pH 2 and pH 6 indicates that the functional groups are disordered. At pH 2, a slightly disordered backbone (compared to pH 4) results in a disordered pendant group exhibiting no measurable VSFSS signal. While at pH 4, the highly ordered backbone contributes to minor organization of the carbonyl. In addition to disorder, the lack of signal could be attributed to low surface population as described above. To confirm the presence of a C=O vibrational mode at pH 4, emulsions stabilized with 1000 ppm PAA were measured in the C=O stretching region (Figure S7). A strong feature with good signal to noise with 1000 ppm PAA was measured at the same frequency as the emulsions measured with 500 ppm PAA. These results suggest that the C=O group of PAA at 500 ppm concentration at pH 4 are ordered but lack the interfacial population necessary to elucidate a strong SFG response.

VSFSS measurements in the COO- stretching region were made to determine if the deprotonated functional group is ordered (Fig. 3C). However, no signal was observed in the carboxylate stretching region for any pH conditions. For pH 2 and pH 4, the percent protonation at the interface indicates that the carboxylic acid group is dominating the surface population. Thus, any carboxylate groups, if present, are in too little in population to be visible by VSFSS and/or not well ordered. At pH 6, although the polymer is significantly deprotonated and COO- groups are present (~16.7 % protonation), the polymer is predominately solvated in the water phase as suggested by low surface pressure (<10 mN/m) measured by pendant drop surface tensiometery data (Figure S3). Therefore, there will be no carboxylate organization at the interface, consistent with the conclusions suggested above by surface tension and VSFSS C-H region data and with VSFS experiments at the CCl<sub>4</sub>/water planar interface [37].

The adsorption of PAA to the hexadecane/water interface can also be rationalized by the hydrophilic-lipophilic balance (HLB), a metric commonly used for surfactants to describe their relative oil or water solubility. Surfactants with a lower HLB value (closer to 0) have better oil solubility while surfactants with a higher HLB value (closer to 20) exhibit better water solubility. Generally, oil in water emulsifiers have an HLB between 8 and 16. Using the methods proposed by Davies [77], we calculated HLB values for PAA at pH 2, 4, and 6 using our experimentally derived % protonation values (Eq. 2 Supporting Information). We found that at pH 2 and 4, PAA has an HLB or 8.17 and 8.97, respectively, indicating that the polymer is fairly oil-soluble and acts as a good oil-in-water emulsifier. However, the HLB value for PAA at pH 6 is 22.3 suggesting that the polymer does not have sufficient surfactant characteristics and prefers to be solubilized in water, consistent with our spectroscopic analysis.

From these results exploring PAA at the emulsion interface at pH conditions with low deprotonation (<5 %), it appears that sterics play a significant role in dictating the colloidal stability of these emulsions as the electrostatic repulsion and consequential colloidal stability experienced in this system is not what would be predicted by DLVO theory. Emulsions prepared at pH 2, despite having almost zero surface charge are colloidally stable, while pH 6 oil droplets have a high surface charge but are unstable. At pH 4, the natural pH of the system, the polymer is largely protonated (~95 %), has high surface pressure, and was a wellordered chain at the interface. Presumably, the CH backbone is aligned into the oil phase while the carboxylic acid groups are slightly aligned in the water phase. With the addition of acid ( $\sim$ 99 % protonation at pH 2), PAA is still present at the interface in high population but experiences less chain organization as compared to pH 4 due to intramolecular hydrogen bonding between acid groups and subsequent coiling of the polymer. On the other hand, at pH 6 ( $\sim$ 17 % protonated) the polymer is not ordered at the interface and a higher population of the polymer prefers to be solvated in the water phase as an extended, charged chain. Fig. 6 summarizes the molecular picture of PAA-coated oil droplets.

#### 3.3. Addition of salt to PAA-stabilized emulsions

In an effort to charge screen PAA and promote interfacial activity, in particular for pH 6, the impact of chloride salts on emulsion stability was studied. Upon the addition of chloride-based cations, the size, PDI, and zeta-potential of PAA-stabilized emulsions were measured (Fig. 4). Concentrations of salt ranged from 0 to 2 mM for the divalent cations (Ca<sup>2+</sup> and Mg<sup>2+</sup>) and 0-6 mM for the monovalent cations (Na<sup>+</sup> and NH<sub>4</sub><sup>+</sup>) to keep the ionic strength of the solution consistent between varying cations. In general, the addition of salt causes minor changes to the size or PDI of the emulsion. To ensure consistent normalization of the scattered light generated and collected from VSFSS experiments, colloid radius must be within 100-900 nm [78]. At pH 2 and pH 4, emulsions generally stayed within this size regime except for the addition of NaCl at high concentrations at pH 2 which could be attributed to PAA crowding at the interface. At pH 2 and pH 4, PDI exhibits no trend with the addition of salt. The negligible change in size or PDI of the emulsions at pH 2 and pH 4 with the addition of salt suggests that no additional polymer layers are absorbed to the surface. At pH 6, size and PDI change drastically but without any clear trend. The wide range in these values are attributed to unstable emulsions that contain little, if any, polymer at the interface, and do not favorably stabilize the oil droplets. These results suggest that the salt ions do not bring pH 6 polymer to the surface as observed at the planar interface, which could be attributed to the different chemical nature of the interfaces and solubility of CCl<sub>4</sub> [37].

In all pH conditions the addition of salt causes a reduction in the magnitude of the zeta potential. This is most noticeable at pH 4 and pH 6 where charge screening reduces the zeta potential by almost 20 mV with the addition of only 0.3 mM ionic strength salt. Significant charge screening occurs for ionic strengths up to  $\sim\!1.5$  mM before the zeta potential plateaus with the addition of salt up to 6 mM ionic strength. Despite the addition of salt and subsequent charge screening, the pH 6 oil droplets are never stabilized, as evident by the large diameter and high PDI. This suggests that at pH 6, even with charge screening at the interface promoting the zeta potential akin to stable pH 4 emulsions (<30 mV), the polymer would rather be solvated in the water phase than oriented at the interface.

To better understand how the presence of salt impacts polymer conformation and promotes charge screening, VSFSS studies were conducted on PAA-coated colloids with the addition of the various salts. An ionic strength of 2 mM was chosen for all VSFSS salt studies because emulsions stabilized with CaCl<sub>2</sub> at 2 mM ionic strength (1 mM CaCl<sub>2</sub>) exhibited the most stable size and PDI at pH 6 and because charge screening plateaus by 2 mM ionic strength. Upon the addition of 2 mM ionic strength salt, the VSFSS intensity of PAA in the CH stretching region decreases at pH 4 to a signal intensity on the same scale as emulsions at pH 2 (Figs. 5A, 5B). At pH 2, adding NaCl and NH<sub>4</sub>Cl promotes a slight change in the overall intensity, while at pH 6, no spectral features are observed with added salt (Fig. 5C). A small population of PAA does adsorb to the interface at pH 6 with the addition of salt, as observed through interfacial pressure data (Figure S3), suggesting that salt decreases the hydrophilic character of the carboxylic acid group therefore reducing the HLB (Supporting Information) and promoting surface adsorption. However, as seen spectroscopically, the addition of salt does not cause ordering of the polymer chain at the interface. The VSFSS response of the carbonyl group was also measured with the addition of 2 mM ionic strength salt however no increase in signal was observed (Figure S8). Peak position shifts are potentially present in the C=O spectra, however the signal to noise is so low in this region that no conclusions can be made with confidence.

In general, adding salt changes the structure of the polymer at pH 4 more drastically than at pH 2 as more of the polymer is deprotonated at pH 4 and thus there are more carboxylate sites for the cations to bind. The binding of the cation to carboxylate sites disrupts polymer organization at the surface as the polymer likely needs to readjust and coil at the confined emulsion interface to create cationic bridging between acid

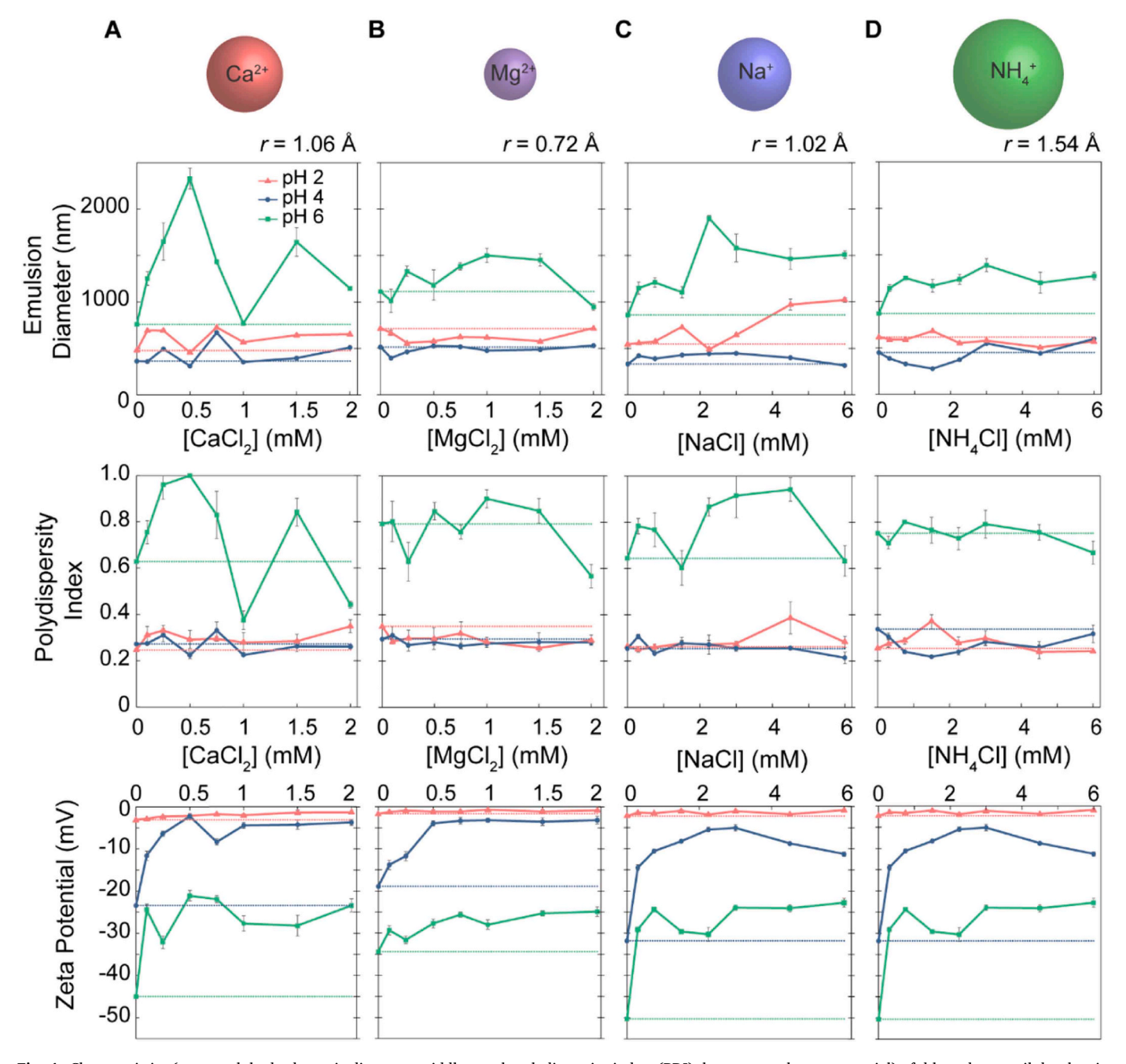


Fig. 4. Characteristics (top panel: hydrodynamic diameter, middle panel: polydispersity index, (PDI), bottom panel: zeta potential) of d-hexadecane oil droplets in  $D_2O$  stabilized with 500 ppm PAA at varying pH conditions with the addition of A)  $CaCl_2$ , B)  $MgCl_2$ , C) Colored NaCl, and D) Colored lines are a guide to the eye for emulsions made without salt.

groups [73]. As best exemplified in the pH 4 condition, the addition of salt promotes the polymer to develop a more random coil backbone conformation, that mimics that of the natural pH 2 polymer, resulting in a decrease in the VSFSS signal with the addition of salt. The impact of chloride counterion at the surface can be neglected due to the inherent negative zeta potential of PAA-stabilized emulsions without salt. With the addition of chloride salts, the surface charge is reduced in magnitude suggesting that the cations are more attracted to the negatively charged interface than the anions which are assumed to be solvated in the water phase.

A quantitative look at the VSFSS spectral changes with addition of salt shows that as the electronegativity of the cation increases, as determined by the Pauling scale, we see a corresponding decrease in  $\text{CH}_2$  integrated area and zeta potential magnitude (Figs. 5D, 5E). The  $\text{CH}_2$ 

area was calculated by integrating the area from the full width half max of a Gaussian fit of the  $\mathrm{CH}_2$  feature centered around 2930  $\mathrm{cm}^{-1}.$  As  $\mathrm{NH}_+^+$  is a molecular ion and does not have electronegativity, it is excluded from this trend. The decreasing  $\mathrm{CH}_2$  intensity with increasing electronegativity is present regardless of pH but is clearer at pH 4 due to the higher number of carboxylic acid groups available to interact with the cations. As the electronegativity of the cation increases, it has an increased ability to pull the electron density away from the carboxylic acid groups on the polymer and promote solvation in the water phase. Cations with a higher electronegativity promote polymer coiling, as demonstrated by the decrease in CH signal intensity and effectively charge screening the zeta potential. This results in a disruption of the CH backbone conformation and a decrease in the polymer persistence length at pH 4 (Fig. 6, bottom). Slight change in the polymer structure is

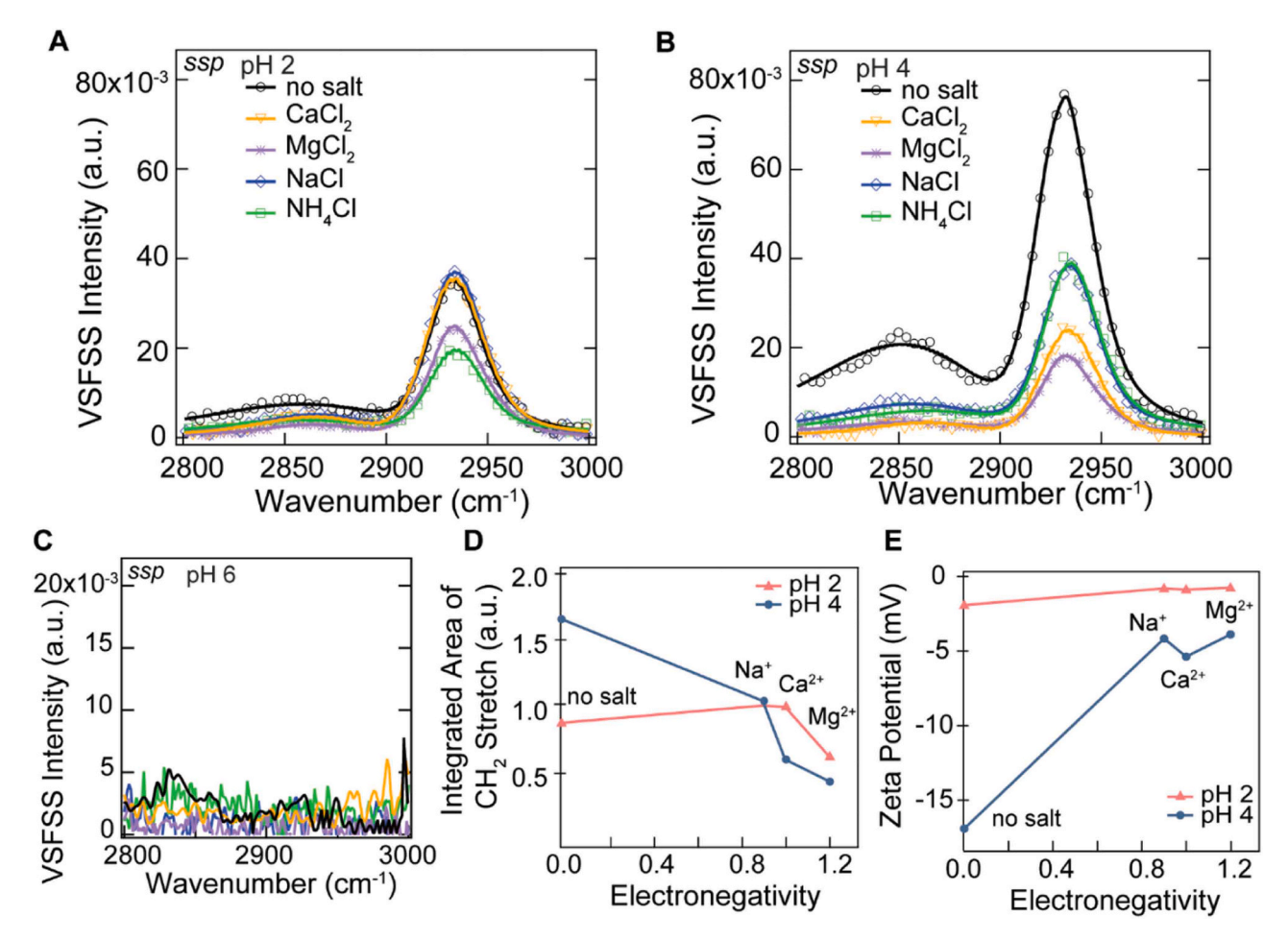


Fig. 5. VSFSS (ssp polarization) of d-hexadecane oil droplets in  $D_2O$  stabilized with 500 ppm PAA and 2 mM ionic strength salt at A) pH 2, B) pH 4, and C) pH 6. Solid lines represent fits of the data. Electronegativity of cations defined by the Pauling scale are compared to D) the integrated area of the  $CH_2$  stretch and E) zeta potential.

observed at pH 2 due to the minimal population of carboxylate groups that can interact with the cation (Fig. 6, bottom).

The absence of signal from PAA with salt at pH 6 are in contrast with observations at the planar oil/water interface where the addition of salt increased the C=O signal and had negligible impact on the CH stretching modes. At a planar interface, the dynamics of adsorbed molecules are dominated by the thermodynamics of positive enthalpic interactions while slightly limited by kinetic diffusion through the medium. Thus, over time, a polymer at the planar oil/water interface can stretch and extend to adopt a thermodynamically favorable state that allows for stabilizing complexation with metal cations. Despite the significant charge screening exhibited at pH 6, the absence of VSFSS signal suggests that PAA is not complexing with ions at the oil droplet interface. Independent of pH or salt addition, in the kinetically trapped emulsion system, the adsorbed PAA layer will adopt a thermodynamically stable orientation that is different from that at the planar interface due to the competing kinetic energy driving oil droplets to coalescence. To carefully consider molecular adsorption at interfaces, we cannot neglect how the factors that contribute to colloidal stability, namely sterics and charge, impact the conformation of the surface-active species. The competition between polymer adsorption and droplet coalescence has implications on molecular structure when variables such as pH and ionic strength are varied. For PAA at pH 6 at the oil/water droplet interface, the energy released from droplet aggregation overcomes the slight polymer adsorption that is present with the addition of cations and the polymer remains solvated in the aqueous phase (Fig. 6, bottom). However, PAA at pH 2 and pH 4 can stabilize emulsions through sterics alone due to the adsorption of the highly surface-active protonated polymer. It is likely that other charged macromolecules, such as proteins, can stabilize colloids through a steric layer in the same manner.

## 4. Conclusions

The interface-specific vibrational spectroscopy employed here along with complementary emulsion characteristic measurements provides a molecular-level picture of PAA at the hexadecane/water emulsion interface, which has previously been explored only at planar interfaces. VSFSS spectra in the CH stretching region suggest an ordered PAA backbone at pH 2 and pH 4 (Fig. 6), while at pH 6, the polymer prefers to be solvated in the aqueous phase with minimal, disordered chain adsorption. With the addition of salt, no PAA adsorption was observed at pH 6 which contrasts with findings at the planar CCl<sub>4</sub>/water interface where salt addition promotes polymer adsorption. While the addition of salt causes charge screening at the hexadecane/water emulsion interface, the pH 6 polymer does not become more interfacially ordered resulting in a unstable colloid. At pH 2, the influence of cations has minimal impact on the conformation of PAA due to the low % protonation, however, at pH 4, the addition of salt causes a decrease in persistence length and increase in polymer coiling, resulting in an ordered backbone that mimics the conformational structure of the pH 2 polymer. While there have been previous reports of sterically-stabilized emulsions, our results provide a molecular level understanding of the stability mechanism.

Due to the kinetically trapped state of emulsions as compared to the

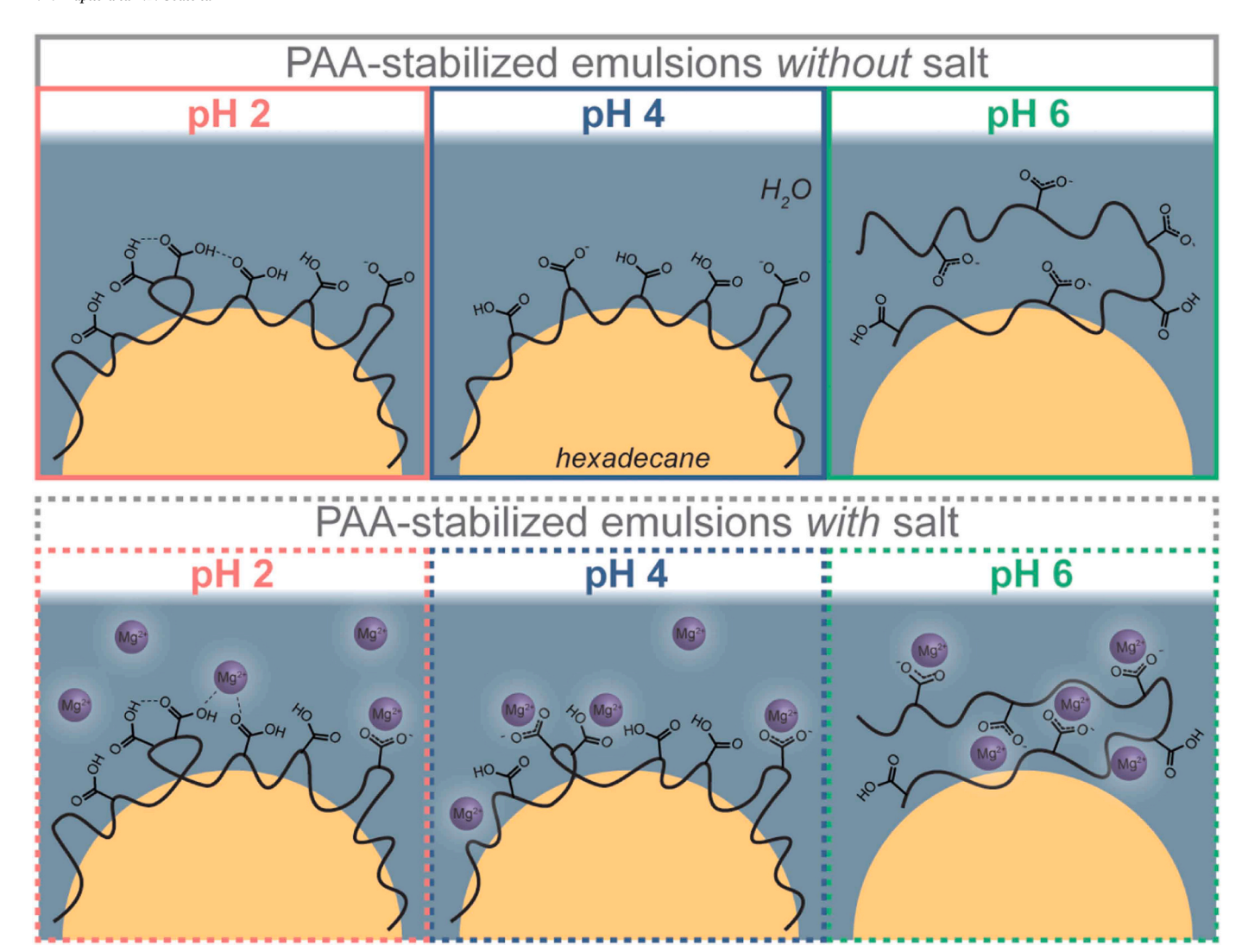


Fig. 6. Illustration depicting the behavior of PAA at the hexadecane/water droplet interface in varying pH conditions without (above) and with (below) the presence of salt, the example of MgCl<sub>2</sub> shown here. Chloride anions have been omitted for clarity and are solvated in the water phase.

thermodynamically stable planar interface, polymer conformation and colloidal stability are closely intertwined. While classical DLVO theory suggests that a large surface charge is necessary to stabilize colloids, these results show that a surface active, steric layer is enough to maintain emulsion stability for upwards of 1 week at pH 2 and pH 4, while too much charge on the polyelectrolyte (at pH 6) causes unstable oil droplets with polymers solvated in the bulk phase. Future work includes varying polymer molecular weight to carefully tune the steric character, with the intention that polymers of a very low molecular weight could behave like surfactants. Additionally, this work provides a basis for understanding other pH-dependent polymers, such as those stable in a basic regime. In particular, emulsion stability via pH-tunable polymers can be applied to targeted drug delivery, allowing for dissolution of a drug in specific conditions. Ultimately, the ability to stabilize emulsions with a polymer alone aids in forming colloidally stable systems, such as those coated by proteins coronas or polymer coacervates and broadens our understanding of traditional DLVO theory.

## **Funding sources**

This material is based upon work supported by the National Science Foundation under Grant No CHE 2003526.

### Associated content

Supporting Information is available and contains percent protonation calculation, emulsion stability characterization, surface tension measurements, additional VSFS spectra, and fitting parameters.

## **Declaration of Competing Interest**

The authors declare that they have no known competing financial interests or personal relationships that could have appeared to influence the work reported in this paper.

## **Data Availability**

Data will be made available on request.

## Acknowledgements

Thank you to Geraldine Richmond and Emma Tran for inspiration and advice during the conceptualization of this work. Thank you to Fred G. Moore for the fitting routine algorithms. Thanks to Konnor Jones, Andrew Carpenter, and Priscilla Lewis with assistance in editing and processing the manuscript.

#### Appendix A. Supporting information

Supplementary data associated with this article can be found in the online version at doi:10.1016/j.colsurfa.2024.134414.

#### References

- [1] A. Gupta, H.B. Eral, T.A. Hatton, P.S. Doyle, Nanoemulsions: formation, properties and applications, Soft Matter 12 (11) (2016) 2826–2841, https://doi.org/10.1039/
- [2] D.J. McClements, Nanoemulsions versus microemulsions: terminology, differences, and similarities, Soft Matter 8 (6) (2012) 1719–1729, https://doi.org/10.1039/ C2SM06903B
- [3] B. Ding, S.H. Ahmadi, P. Babak, S.L. Bryant, A. Kantzas, On the stability of pickering and classical nanoemulsions: theory and experiments, Langmuir 39 (20) (2023) 6975–6991, https://doi.org/10.1021/acs.langmuir.3c00133.
- [4] N. Anton, T.F. Vandamme, Nano-emulsions and micro-emulsions: clarifications of the critical differences, Pharm. Res 28 (5) (2011) 978–985, https://doi.org/ 10.1007/s11095-010-0309-1.
- [5] V. John, C. Arnosti, J. Field, E. Kujawinski, A. McCormick, The role of dispersants in oil spill remediation: fundamental concepts, rationale for use, fate, and transport issues, Oceanography 29 (3) (2016) 108–117.
- [6] M.F. Attia, S.M. Dieng, M. Collot, A.S. Klymchenko, C. Bouillot, C.A. Serra, M. Schmutz, M. Er-Rafik, T.F. Vandamme, N. Anton, Functionalizing nanoemulsions with carboxylates: impact on the biodistribution and pharmacokinetics in mice, Macromol. Biosci. 17 (7) (2017) 1600471, https://doi.org/10.1002/mabi.201600471.
- [7] B.J.D. Le Révérend, M.S. Taylor, I.T. Norton, Design and application of water-in-oil emulsions for use in lipstick formulations, Int. J. Cosmet. Sci. 33 (3) (2011) 263–268, https://doi.org/10.1111/j.1468-2494.2010.00624.x.
- [8] T.G. Mason, J.N. Wilking, K. Meleson, C.B. Chang, S.M. Graves, Nanoemulsions: formation, structure, and physical properties, J. Phys. Condens. Matter 18 (41) (2006) R635–R666, https://doi.org/10.1088/0953-8984/18/41/R01.
- E.B. Kujawinski, C.M. Reddy, R.P. Rodgers, J.C. Thrash, D.L. Valentine, H.K. White, The first decade of scientific insights from the deepwater horizon oil release, Nat. Rev. Earth Environ. 1 (5) (2020) 237–250, https://doi.org/10.1038/s43017-020-0046-x
- [10] D.K. Beaman, E.J. Robertson, G.L. Richmond, From head to tail: structure, solvation, and hydrogen bonding of carboxylate surfactants at the organic–water interface, J. Phys. Chem. C. 115 (25) (2011) 12508–12516, https://doi.org/10.1021/jp202061v.
- [11] P. Balzerowski, K. Meister, J. Versluis, H.J. Bakker, Heterodyne-detected sum frequency generation spectroscopy of polyacrylic acid at the air/water-interface, Phys. Chem. Chem. Phys. 18 (4) (2016) 2481–2487, https://doi.org/10.1039/ C5CP06177F.
- [12] E. Zdrali, Y. Chen, H.I. Okur, D.M. Wilkins, S. Roke, The molecular mechanism of nanodroplet stability, ACS Nano 11 (12) (2017) 12111–12120, https://doi.org/ 10.1021/acsnano.7b05100.
- [13] N. Smolentsev, W.J. Smit, H.J. Bakker, S. Roke, The interfacial structure of water droplets in a hydrophobic liquid, Nat. Commun. 8 (1) (2017) 15548, https://doi. org/10.1038/ncomms15548.
- [14] M.J. Foster, A.P. Carpenter, G.L. Richmond, Dynamic duo: vibrational sum frequency scattering investigation of ph-switchable carboxylic acid/carboxylate surfactants on nanodroplet surfaces, J. Phys. Chem. B 125 (33) (2021) 9629–9640, https://doi.org/10.1021/acs.jpcb.1c05508.
- [15] J.C. Athas, K. Jun, C. McCafferty, O. Owoseni, V.T. John, S.R. Raghavan, An effective dispersant for oil spills based on food-grade amphiphiles, Langmuir 30 (31) (2014) 9285–9294, https://doi.org/10.1021/la502312n.
- [16] J.S. Gebauer, M. Malissek, S. Simon, S.K. Knauer, M. Maskos, R.H. Stauber, W. Peukert, L. Treuel, Impact of the nanoparticle–protein corona on colloidal stability and protein structure, Langmuir 28 (25) (2012) 9673–9679, https://doi. org/10.1021/la301104a.
- [17] C. Vasti, D.A. Bedoya, R. Rojas, C.E. Giacomelli, Effect of the protein corona on the colloidal stability and reactivity of LDH-based nanocarriers, J. Mater. Chem. B 4 (11) (2016) 2008–2016, https://doi.org/10.1039/C5TB02698A.
- [18] Tengjisi, Y. Hui, Y. Fan, D. Zou, G.H. Talbo, G. Yang, C.-X. Zhao, Influence of nanoparticle mechanical property on protein corona formation, J. Colloid Interface Sci. 606 (2022) 1737–1744, https://doi.org/10.1016/j.jcis.2021.08.148.
- [19] J. Ren, N. Andrikopoulos, K. Velonia, H. Tang, R. Cai, F. Ding, P.C. Ke, C. Chen, Chemical and biophysical signatures of the protein corona in nanomedicine, J. Am. Chem. Soc. 144 (21) (2022) 9184–9205, https://doi.org/10.1021/jacs.2c02277.
- [20] A.S. Chatterley, T.W. Golbek, T. Weidner, Measuring protein conformation at aqueous interfaces with 2D infrared spectroscopy of emulsions, J. Phys. Chem. Lett. 13 (31) (2022) 7191–7196, https://doi.org/10.1021/acs.jpclett.2c01324.
- [21] T.W. Golbek, K. Strunge, A.S. Chatterley, T. Weidner, Peptide orientation at emulsion nanointerfaces dramatically different from flat surfaces, J. Phys. Chem. Lett. 13 (46) (2022) 10858–10862, https://doi.org/10.1021/acs.jpclett.2c02870.
- [22] M.P. Andersson, M.H.M. Olsson, S.L.S. Stipp, Predicting the pKa and stability of organic acids and bases at an oil-water interface, Langmuir 30 (22) (2014) 6437–6445, https://doi.org/10.1021/la5008318.
- [23] B.A. Wellen, E.A. Lach, H.C. Allen, Surface pKa of octanoic, nonanoic, and decanoic fatty acids at the air–water interface: applications to atmospheric aerosol chemistry, Phys. Chem. Chem. Phys. 19 (39) (2017) 26551–26558, https://doi. org/10.1039/C7CP04527A.

- [24] C.J. Drummond, F. Grieser, T.W. Healy, Acid-base equilibria in aqueous micellar solutions. part 1.—'simple' weak acids and bases, J. Chem. Soc., Faraday Trans. 1 85 (3) (1989) 521–535, https://doi.org/10.1039/F19898500521.
- [25] S.M. Copp, R.L. Hamblin, K. Swingle, D. Rai, V.S. Urban, S.A. Ivanov, G. A. Montaño, Complex pH-dependent interactions between weak polyelectrolyte block copolymer micelles and molecular fluorophores, Langmuir 38 (6) (2022) 2038–2045, https://doi.org/10.1021/acs.langmuir.1c02889.
- [26] M. Houska, E. Brynda, Interactions of proteins with polyelectrolytes at solid/liquid interfaces: sequential adsorption of albumin and heparin, J. Colloid Interface Sci. 188 (2) (1997) 243–250, https://doi.org/10.1006/jcis.1996.4576.
- [27] B.N. Dickhaus, R. Priefer, Determination of polyelectrolyte pka values using surface-to-air tension measurements, Colloids Surf. A Physicochem. Eng. Asp. 488 (2016) 15–19, https://doi.org/10.1016/j.colsurfa.2015.10.015.
- [28] A.M. Rumyantsev, N.E. Jackson, J.J. de Pablo, Polyelectrolyte complex coacervates: recent developments and new frontiers, Annu. Rev. Condens. Matter Phys. 12 (1) (2021) 155–176, https://doi.org/10.1146/annurev-conmatphys-042020.113457
- [29] K.O. Margossian, M.U. Brown, T. Emrick, M. Muthukumar, Coacervation in polyzwitterion-polyelectrolyte systems and their potential applications for gastrointestinal drug delivery platforms, Nat. Commun. 13 (1) (2022) 2250, https://doi.org/10.1038/s41467-022-29851-y.
- [30] N. Tanaka, H. Kitano, N. Ise, Raman spectroscopic study of hydrogen bonding in aqueous carboxylic acid solutions. 3. polyacrylic acid, Macromolecules 24 (10) (1991) 3017–3019, https://doi.org/10.1021/ma00010a060.
- [31] T. Swift, L. Swanson, M. Geoghegan, S. Rimmer, The pH-responsive behaviour of poly(acrylic acid) in aqueous solution is dependent on molar mass, Soft Matter 12 (9) (2016) 2542–2549, https://doi.org/10.1039/C5SM02693H.
- [32] D.G. Mintis, V.G. Mavrantzas, Effect of pH and molecular length on the structure and dynamics of short poly(acrylic acid) in dilute solution: detailed molecular dynamics study, J. Phys. Chem. B 123 (19) (2019) 4204–4219, https://doi.org/ 10.1021/acs.jpcb.9b01696.
- [33] R. Chollakup, J.B. Beck, K. Dirnberger, M. Tirrell, C.D. Eisenbach, Polyelectrolyte molecular weight and salt effects on the phase behavior and coacervation of aqueous solutions of poly(acrylic acid) sodium salt and poly(allylamine) hydrochloride, Macromolecules 46 (6) (2013) 2376–2390, https://doi.org/ 10.1021/ma2021720.
- [34] Z. Gong, N.S. Zacharia, B.D. Vogt, Sodium dodecyl sulfate modulates the structure and rheological properties of pluronic F108–Poly(Acrylic Acid) Coacervates), Soft Matter 18 (2) (2022) 340–350. https://doi.org/10.1039/D1SM01273H.
- [35] D.K. Beaman, E.J. Robertson, G.L. Richmond, Unique assembly of charged polymers at the oil—water interface, Langmuir 27 (6) (2011) 2104–2106, https://doi.org/10.1021/la104390u.
- [36] D.K. Beaman, E.J. Robertson, G.L. Richmond, Ordered polyelectrolyte assembly at the oil-water interface, Proc. Natl. Acad. Sci. 109 (9) (2012) 3226–3231, https://doi.org/10.1073/pnas.1200244109.
- [37] D.K. Beaman, E.J. Robertson, G.L. Richmond, Metal ions: driving the orderly assembly of polyelectrolytes at a hydrophobic surface, Langmuir 28 (40) (2012) 14245–14253, https://doi.org/10.1021/la302917p.
- [38] E.J. Robertson, G.L. Richmond, Molecular insights in the structure and layered assembly of polyelectrolytes at the oil/water interface, J. Phys. Chem. C. 118 (49) (2014) 28331–28343, https://doi.org/10.1021/jp5068022.
   [39] B.V. Derjaguin, N.V. Churaev, V.M. Muller, The
- [39] B.V. Derjaguin, N.V. Churaev, V.M. Muller, The Derjaguin—Landau—Verwey—Overbeek (DLVO) theory of stability of lyophobic colloids, in: B.V. Derjaguin, N.V. Churaev, V.M. Muller (Eds.), In Surface Forces, Springer US, Boston, MA, 1987, pp. 293–310, https://doi.org/10.1007/978-1-4757-6639-4 8.
- [40] H.T. Phan, A.J. Haes, What does nanoparticle stability mean? J. Phys. Chem. C. 123 (27) (2019) 16495–16507, https://doi.org/10.1021/acs.jpcc.9b00913.
- [41] S.J. Hunter, S.P. Armes, Pickering emulsifiers based on block copolymer nanoparticles prepared by polymerization-induced self-assembly, Langmuir 36 (51) (2020) 15463–15484, https://doi.org/10.1021/acs.langmuir.0c02595.
- [42] K. Chen, S. Wang, X. Guo, Confinement effect on the aqueous behaviors of free poly (acrylic acid) and poly(acrylic acid) grafted on a nanoparticle surface, Colloid Polym. Sci. 297 (9) (2019) 1223–1231, https://doi.org/10.1007/s00396-019-04541-2
- [43] E. Tran, A.P. Carpenter, G.L. Richmond, Probing the molecular structure of coadsorbed polyethylenimine and charged surfactants at the nanoemulsion droplet surface, Langmuir 36 (31) (2020) 9081–9089, https://doi.org/10.1021/acs. langmuir.0c01095.
- [44] Y.L. Fan, C.H. Tan, Y. Lui, D. Zudhistira, S.C.J. Loo, Mechanistic formation of drugencapsulated janus particles through emulsion solvent evaporation, RSC Adv. 8 (29) (2018) 16032–16042, https://doi.org/10.1039/C8RA02271B.
- [45] M. Nandy, B.B. Lahiri, J. Philip, Probing concentration and time dependent conformational changes in poly acrylic acid stabilized magnetic nanoemulsion using magnetic chaining-based inter-droplet force measurement, Colloid Interface Sci. Commun. 47 (2022) 100592, https://doi.org/10.1016/j.colcom.2022.100592.
- [46] S. Han, H. An, H. Tao, L. Li, Y. Qi, Y. Ma, X. Li, R. Wang, J. Zhang, Advanced emulsions via noncovalent interaction-mediated interfacial self-assembly, Chem. Commun. 54 (25) (2018) 3174–3177, https://doi.org/10.1039/C8CC00016F.
- [47] D. Liu, Z. Zhang, K. Zhang, Y. Li, D.-P Song, Host-Guest interaction mediated interfacial co-assembly of cyclodextrin and bottlebrush surfactants for precisely tunable photonic supraballs, Small n/a (n/a) (2024) 2312099, https://doi.org/ 10.1002/smll.202312099.
- [48] A. Krężel, W. Bal, A formula for correlating pKa values determined in D2O and H2O, J. Inorg. Biochem. 98 (1) (2004) 161–166, https://doi.org/10.1016/j. jinorgbio.2003.10.001.

- [49] W.I. Goldburg, Dynamic light scattering, Am. J. Phys. 67 (12) (1999) 1152–1160, https://doi.org/10.1119/1.10101
- [50] J.D. Clogston, A.K. Patri, Zeta potential measurement, Methods Mol. Biol. 697 (2011) 63–70, https://doi.org/10.1007/978-1-60327-198-1 6.
- [51] W. Xi, A.J. Haes, Elucidation of HEPES affinity to and structure on gold nanostars, J. Am. Chem. Soc. 141 (9) (2019) 4034–4042, https://doi.org/10.1021/ iacs.8b13211.
- [52] Y.R. Shen, Surface properties probed by second-harmonic and sum-frequency generation, Nature 337 (6207) (1989) 519–525, https://doi.org/10.1038/ 337519a0.
- [53] A.G. Lambert, P.B. Davies, D.J. Neivandt, Implementing the theory of sum frequency generation vibrational spectroscopy: a tutorial review, Appl. Spectrosc. Rev. 40 (2) (2005) 103–145, https://doi.org/10.1081/ASR-200038326.
- [54] E. Tran, K.K. Jones, G.A. Cano, F.G. Moore, L.F. Scatena, Spectroscopic studies of zwitterionic DDAPS at planar and droplet oil/water interfaces, J. Phys. Chem. B 126 (39) (2022) 7720–7730, https://doi.org/10.1021/acs.jpcb.2c02664.
- [55] NLS-Simulate. Get the software safely and easily. Software Informer. (https://nls-simulate.software.informer.com/) (Accessed 2022-06-06).
- [56] A.G.F. Beer, S. de; Roke, J.I. Dadap, Theory of optical second-harmonic and sum-frequency scattering from arbitrarily shaped particles, J. Opt. Soc. Am. B, JOSAB 28 (6) (2011) 1374–1384, https://doi.org/10.1364/JOSAB.28.001374.
- [57] C.D. Bain, P.B. Davies, T.Hui Ong, R.N. Ward, M.A. Brown, Quantitative analysis of monolayer composition by sum-frequency vibrational spectroscopy, Langmuir 7 (8) (1991) 1563–1566, https://doi.org/10.1021/la00056a003.
- [58] K. Roger, B. Cabane, Why are hydrophobic/water interfaces negatively charged? Angew. Chem. Int. Ed. 51 (23) (2012) 5625–5628, https://doi.org/10.1002/anje.201108228
- [59] A.P. Carpenter, E. Tran, R.M. Altman, G.L. Richmond, Formation and surfacestabilizing contributions to bare nanoemulsions created with negligible surface charge, Proc. Natl. Acad. Sci. USA 116 (19) (2019) 9214–9219, https://doi.org/ 10.1073/nnas.1900802116
- [60] E. Tran, G.L. Richmond, Interfacial steric and molecular bonding effects contributing to the stability of neutrally charged nanoemulsions, Langmuir 37 (43) (2021) 12643–12653, https://doi.org/10.1021/acs.langmuir.1c02020.
- [61] S. Barany, Polymer adsorption and electrokinetic potential of dispersed particles in weak and strong electric fields, Adv. Colloid Interface Sci. 222 (2015) 58–69.
- [62] I. Ostolska, M. Wiśniewska, Application of the zeta potential measurements to explanation of colloidal Cr2O3 stability mechanism in the presence of the ionic polyamino acids, Colloid Polym. Sci. 292 (10) (2014) 2453–2464, https://doi.org/ 10.1007/s00396-014-3276-y.
- [63] Nobbmann, U. Polydispersity what does it mean for DLS and chromatography? -Materials Talks. (https://www.materials-talks.com/polydispersity-what-does-it-mean-for-dls-and-chromatography/) (Accessed 2024-01-29).
- [64] M. Rolland, N.P. Truong, K. Parkatzidis, E.H. Pilkington, A.L. Torzynski, R. W. Style, E.R. Dufresne, A. Anastasaki, Shape-controlled nanoparticles from a low-energy nanoemulsion, JACS Au 1 (11) (2021) 1975–1986, https://doi.org/10.1021/jacsau.1c00321.
- [65] D. To, G. Kali, S. Haddadzadegan, A.M. Jörgensen, K. Nigl, F. Ricci, A. Bernkop-Schnürch, Power-up for mucoadhesiveness: two generations of thiolated

- surfactants for enhanced sticky nanoemulsions, ACS Biomater. Sci. Eng. 9 (12) (2023) 6797–6804, https://doi.org/10.1021/acsbiomaterials.3c01207.
- [66] Y. Guo, X. Zhang, X. Wang, L. Zhang, Z. Xu, D. Sun, Nanoemulsions stable against ostwald ripening, Langmuir 40 (2) (2024) 1364–1372, https://doi.org/10.1021/ acc.langmuir 3c03019
- [67] M. Chen, X. Liu, A. Fahr, Skin penetration and deposition of carboxyfluorescein and temoporfin from different lipid vesicular systems: in vitro study with finite and infinite dosage application, Int. J. Pharm. 408 (1) (2011) 223–234, https://doi. org/10.1016/j.ijpharm.2011.02.006.
- [68] M. Danaei, M. Dehghankhold, S. Ataei, F. Hasanzadeh Davarani, R. Javanmard, A. Dokhani, S. Khorasani, M.R. Mozafari, Impact of particle size and polydispersity index on the clinical applications of lipidic nanocarrier systems, Pharmaceutics 10 (2) (2018) 57, https://doi.org/10.3390/pharmaceutics10020057.
- [69] R. Meng, C. Wang, J. Jin, R. Wang, L. Deng, Self-assembly of hydrophobically associating amphiphilic polymer with surfactant and its effect on nanoemulsion, Colloids Surf. A: Physicochem. Eng. Asp. 642 (2022) 128599, https://doi.org/ 10.1016/j.colsurfa.2022.128599.
- [70] D.A. Estabrook, A.F. Ennis, R.A. Day, E.M. Sletten, Controlling nanoemulsion surface chemistry with poly(2-oxazoline) amphiphiles, Chem. Sci. 10 (14) (2019) 3994–4003, https://doi.org/10.1039/C8SC05735D.
- [71] S.J. Hunter, E.J. Cornel, O.O. Mykhaylyk, S.P. Armes, Effect of salt on the formation and stability of water-in-oil pickering nanoemulsions stabilized by diblock copolymer nanoparticles, Langmuir 36 (51) (2020) 15523–15535, https:// doi.org/10.1021/acs.langmuir.0c02742.
- [72] J. Dong, Y. Ozaki, K. Nakashima, FTIR Studies of conformational energies of poly (acrylic acid) in cast films, J. Polym. Sci. Part B Polym. Phys. 35 (3) (1997) 507–515, https://doi.org/10.1002/(SICI)1099-0488(199702)35:3<507::AID-POLB9>3.0.C0:2-0.
- [73] D. Hu, Z. Yang, K.C. Chou, Interactions of polyelectrolytes with water and ions at air/water interfaces studied by phase-sensitive sum frequency generation vibrational spectroscopy, J. Phys. Chem. C. 117 (30) (2013) 15698–15703, https:// doi.org/10.1021/jp404308g.
- [74] N.A. Valley, E.J. Robertson, G.L. Richmond, Twist and turn: effect of stereoconfiguration on the interfacial assembly of polyelectrolytes, Langmuir 30 (47) (2014) 14226–14233, https://doi.org/10.1021/la5037629.
- [75] Y. Kang, X. Zhao, X. Han, X. Ji, Q. Chen, H. Pasch, A. Lederer, Y. Liu, Conformation and persistence length of chitosan in aqueous solutions of different ionic strengths via asymmetric flow field-flow fractionation, Carbohydr. Polym. 271 (2021) 118402, https://doi.org/10.1016/j.carbpol.2021.118402.
- [76] L. Schmüser, T.W. Golbek, T. Weidner, Windowless detection geometry for sum frequency scattering spectroscopy in the C–D and amide I regions, Biointerphases 16 (1) (2021) 011201, https://doi.org/10.1116/6.0000419.
- [77] Davies, J. T. A quantitative kinetic theory of emulsion type. i. physical chemistry of the emulsifying agent. Gas/liquid and liquid/liquid interfaces, Proc. 2nd Int. Congr. Surf. Act. (1957) 426–438.
- [78] A.G.F. de Beer, S. Roke, Nonlinear mie theory for second-harmonic and sum-frequency scattering, Phys. Rev. B 79 (15) (2009) 155420, https://doi.org/10.1103/PhysRevB.79.155420.